Radiative properties of solvated molecules in dielectric clusters and small particles

Joel Gersten
Department of Physics, City College of the City University of New York, New York, New York 10031
Abraham Nitzan[a)]
Department of Chemical Physics, The Weizmann Institute of Science, Rehovot, 76100, Israel

(Received 10 December 1990; accepted 11 March 1991)

The radiative lifetime of molecules solvated in finite size clusters and particles is studied as a function of size. Four regimes of behavior are indicated by our present and previous theoretical results and by the available experimental data: The microscopic regime (up to a few tens of solvent molecules), where the lifetime is sensitive to microscopic structural details of the cluster; the electrostatic regime (up to sizes $\sim 0.1\lambda$, where λ is the radiation wavelength in the cluster), where the lifetime follows the predictions of classical electrostatics of dielectric environments; the electromagnetic regime (sizes of the order of λ), where the behavior is dominated by electromagnetic resonances in the particles; and the bulk regime (sizes much larger than λ). In the last three regimes the radiative lifetime may be approximated as a product of a cavity factor and a solvent factor. The first depends on the shape of the microscopic cavity surrounding the molecule and the second depends on the shape and size of the solvent particle. For spherical particles and for spherical or mildly spheroidal cavities, the lifetime changes from being longer than that of the free molecule in the electrostatic regime to being shorter in the bulk regime, in agreement with recent experimental results. The transition region occurs in the electrodynamic size regime. In the "bulk regime" (very large particles) molecules near the particle surface (within $\sim$ one wavelength) are strongly affected by electromagnetic Mie resonances and show strong size-dependent deviation from the bulk behavior which characterizes molecules in the interior. The size dependence of the radiative lifetime stands in marked qualitative contrast to the size dependence of the solvent induced frequency shift, which approaches its bulk limit much earlier—when the cluster size becomes much larger than the microscopic cavity size. Finally, the ratio between the integrated absorption profile and the radiative decay rate does not depend on the cluster size.

I. INTRODUCTION

The effect of solvent on the photophysical properties of solvated molecules has been under study for a long time.[1] Similar effects in small clusters are of interest both because of the growing number of optical studies of molecular clusters formed in supersonic beams and because of the characteristic size effects expected in such systems. In two recent articles[2] we and collaborators have presented experimental results on the lifetimes and frequency shifts of 9,10-dichloroanthracene embedded in rare gas clusters, (DCA.X_n; X = Ar, Kr, Xe; prepared by a supersonic free jet expansion of the molecule with the rare gas), and have discussed these results using simple electrostatic theory. An analogous quantum mechanical treatment was recently given by Shalev *et al.*[3] The experimental observations relevant to the present discussion can be summarized as follows:

(a) For small (few atom) clusters the pure radiative lifetime τ_R increases with the number of rare gas atoms, and is then reversed upon adding the next few atoms. A local minimum in τ_R is observed for clusters of 26 Ar atoms.

(b) After these initial changes, the lifetime of clusters of more than about 50 atoms becomes insensitive to further cluster growth, up to the maximal size obtained in this experiment ($\sim$1000 atoms). The lifetime at this 'saturation' is approximately 12% longer than that of the isolated molecule (the latter is 23.3 ns). This should be contrasted with the lifetime observed in bulk (cyclohexane[4]) which is about half that of the free molecule, in accord with expectations based on dielectric theories.

(c) The attachment of rare gas atoms to the dichloroanthracene molecule is accompanied by a red shift which increases monotonically with the cluster size. This dependence saturates at sizes of $\sim$50 atoms, at a value of $\sim$590 cm^{-1} (in Ar), close to that expected for the bulk value.

(d) Both the clustering effects on the lifetime and on the frequency shift correlate with the rare gas polarizability. This correlation is linear for at least the first two attached atoms.

These experimental results have been rationalized[2(b)] in terms of a simple electrostatic model which uses available computed data and some reasonable assumptions for the structure of a few atom clusters, and which takes as a model for the larger clusters a molecule embedded in a dielectric sphere with the dielectric constant of the bulk rare gas. In particular, the initial increase of the radiative lifetime with the first few added atoms was shown to be caused by the polarization induced on atoms occupying the six positions

[a)] On leave from Tel Aviv University, Tel Aviv, Israel.

 0021-9606/91/130686-14$03.00

above and below the rings planes, whose direction from the molecular center is essentially perpendicular to the molecular transition dipole. The following decrease in lifetime is associated with atoms seated close to the molecular plane, above and below the rings, whose distance from the molecular center has a large component parallel to the molecular transition dipole. The minimum observed for τ_R at $n = 26$ (Ar) was interpreted as associated with the completion of a full first solvation layer of Ar atoms around the molecule, and the further increase in τ_R is associated with the start of the buildup of the second layer. The saturation of both lifetime and frequency redshift with cluster sizes of $n \geqslant 50$ is associated with an approximate continuum dielectric behavior, and agrees semiquantitatively[2(b)] with the predictions based on a model of a point dipole embedded in a dielectric sphere with dielectric constant ϵ. Denoting by Γ_R and Γ_R^0 the emission rates for the solvated and the free molecule, respectively, and defining

$$\frac{\Gamma_R}{\Gamma_R^0} \equiv f, \tag{1}$$

a simple electrostatic calculation based on continuum dielectric theory leads to

$$f = \left(\frac{3}{\epsilon + 2}\right)^2, \tag{2}$$

independent of the sphere size and of the location of the dipole in the sphere. The electrostatic limit is valid for $a \ll \lambda = 2\pi c/n\omega$, where a is the particle radius, ω is the radiation frequency, c is the speed of light in vacuum and $n = \sqrt{\epsilon}$ is the refractive index. For Ar ($\epsilon = 1.63$) Eq. (2) yields $f = 0.68$, giving the correct trend but overestimating the experimentally observed factor $\cong 1.12$ for the increase in the radiative emission time.

A possible reason for this discrepancy is the neglect, in Eq. (2) of cavity effects. If, for example, we replace Eq. (2) by

$$f = f_c \cdot f_s, \tag{3}$$

where f_s is given by the right-hand side of (2) and f_c is the cavity correction factor obtained by assuming that the molecule is in a spherical cavity of radius $r \ll a$,

$$f_c = \left(\frac{3}{\epsilon^{-1} + 2}\right)^2 = \frac{9\epsilon^2}{(2\epsilon + 1)^2}. \tag{4}$$

We get (with $\epsilon = 1.63$) $f^{-1} = 1.11$, in remarkable agreement with the experimental observation. The actual result for the cavity effect is however sensitive to the nature of the cavity, its shape and its size (relative to the particle).

While no experimental results are available for the cluster size dependence of the fluorescence line shift and lifetime of molecules embedded in larger dielectric clusters ($n \geqslant 1000$), much work has been done on the effect of bulk dielectric solvent on the spectral shifts, oscillator strength and fluorescence lifetimes of solvated molecules.[5-15] There is a diversity of both experimental and theoretical results, principally related to the fact that the effect of a dielectric medium on the optical properties of an embedded molecule is very sensitive to both short range (cavity structure) and long range (e.g., crystal structure) effects. Thus, relatively straightforward continuum theories[8] are corrected in important ways when a cavity is assumed to exist around the molecule (e.g., Refs. 5 and 10) and further corrections are obtained when the discrete nature of the full solvent matrix is taken into account.[7] Here we limit ourselves to continuum dielectric theory. For a molecule in a bulk solvent this yields Eq. (3), where f_c again depends on the nature of the cavity while f_s is given by[16]

$$f_s = \sqrt{\epsilon}. \tag{5}$$

Equations (3)–(5) with $\epsilon = 1.63$ yield $f^{-1} = 0.6$. This prediction overestimates the solvent effect on the radiative lifetime in comparison to recent experimental results of Crépin and Tramer[17] on the DCA/bulk argon system which give $f^{-1} \sim 0.70$. The fact remains that in small and intermediate size clusters the radiative lifetime is longer, while in the bulk solvent it is shorter, than that of the free molecule. Obviously a crossover from the small particle to the bulk result is expected as the particle size increases.

The aim of the present paper is to examine several aspects of the optical behavior of molecules embedded in spherical particles. In particular we focus on intermediate size and large (relative to λ) particles and examine, within classical electromagnetic theory, the transition from the small particle (electrostatic) limit to the bulk limit. In addition we discuss several models for the cavity correction factor. Together with our previous work on small (few atom) clusters our theoretical results account semiquantitatively for the cluster size dependence of guest molecules.

Section II of this paper reviews the general results for the lifetime of a molecule embedded in a spherical particle for the continuum dielectric model. In Sec. III we examine different results for the cavity correction factor. Section IV includes numerical results and discussion. We conclude in Sec. V.

II. RADIATIVE EMISSION RATES OF A MOLECULE IN A DIELECTRIC SPHERE

The solution of the Maxwell equations with spherical boundary conditions has been carried out by Mie.[18] Application to the problem of a point dipole embedded in a spherical particle (or outside it) was presented by Van der Pol and Bremmer,[19] Kerker and co-workers,[20] Ruppin,[21] Chew,[22] and Leung and George.[23] An equivalent quantum mechanical treatment was carried out by Ching *et al.*[24] However, while general expressions were long available, their implication for our present problem was not studied in detail. In what follows we review the theory that yields the factor f_s of Eq. (1), focusing on particular averages (over molecular orientations and locations) which are the subjects of our discussion.

Consider a dielectric sphere of radius a and dielectric constant ϵ (the magnetic permeability is taken to be 1) in which a single molecule is located at position $\mathbf{R}$. The molecule is represented by a classical point dipole μ, oscillating at frequency ω. The case $\epsilon = 1$ corresponds to the molecule in free space, while $a \to \infty$ is the bulk limit. In this section the molecule is taken to be immersed in the dielectric environment. Modifications of this model by assuming the existence

of a local cavity about the molecule are considered in Sec. III.

Consider first the bulk dielectric limit. In the Lorentz gauge the outgoing solution for the vector potential at a distance $\mathbf{r}$ from an oscillating point dipole is[25]

$$\mathbf{A} = -\frac{i\omega\boldsymbol{\mu}e^{ikr}}{cr}, \tag{6}$$

where c is the speed of light in vacuum and $k=\omega\sqrt{\epsilon}/c$. The scalar potential ϕ, the electric field is $\mathbf{E}$ and the magnetic field $\mathbf{B}$ are given by

$$\begin{aligned}\phi &= (-ic/\epsilon\omega)\nabla\cdot\mathbf{A},\\ \mathbf{E} &= -\nabla\phi + (i\omega/c)\mathbf{A},\\ \mathbf{B} &= \nabla\times\mathbf{A}.\end{aligned} \tag{7}$$

The total outgoing flux P is calculated by integrating the surface normal component of the Poynting vector $\mathbf{S}=(C/8\pi)\mathbf{E}\times\mathbf{B}^*$ over a surface surrounding the dipole. This leads to

$$P\equiv\int \mathbf{S}\cdot d\mathbf{A} = \frac{\omega^4\mu^2\sqrt{\epsilon}}{3c^3}. \tag{8}$$

This is the total power (energy per unit time) radiated by the dipole. As such, this is proportional to the molecule emission rate, which is thus proportional to $\sqrt{\epsilon}$ in this model. The same result is also obtained from a quantum mechanical calculation.[8] We conclude that for a molecule in a continuum bulk dielectric

$$f_s = \sqrt{\epsilon}. \tag{9}$$

Returning to the finite sphere model, we have to calculate the total outgoing power by integrating the Poynting vector over a spherical surface surrounding the sphere. The problem is that of finding the electromagnetic field outside the sphere given an oscillating dipole inside. The general theory is provided in Refs. 19–23 and we only outline the solution procedure and list the results which are needed here. The electric and magnetic fields outside the sphere are written as expansions in vector spherical harmonics

$$\mathbf{E}_{\rm out}(\mathbf{r}) = \sum_{lm}\left\{\frac{i}{q}A_{\rm E}(l,m)\nabla\times[h_l^{(1)}(qr)\mathbf{X}_{lm}] + A_{\rm M}(l,m)h_l^{(1)}(qr)\mathbf{X}_{lm}\right\}, \tag{10a}$$

$$\mathbf{B}_{\rm out}(\mathbf{r}) = \sum_{lm}\left\{A_{\rm E}(l,m)h_l^{(1)}(qr)\mathbf{X}_{lm} - \frac{i}{q}A_{\rm M}(l,m)\nabla\times[h_l^{(1)}(qr)\mathbf{X}_{lm}]\right\}, \tag{10b}$$

where $q=\omega/c$, $k=q\sqrt{\epsilon}$, $\mathbf{X}_{lm}$ are vector spherical harmonics ($\mathbf{X}_{lm}(\hat{r}) = [l(l+1)]^{-1/2}\mathbf{L}Y_{lm}(\hat{r})$, where $\hat{r}\equiv(\phi,\varphi)$, $\mathbf{L}$ is the angular momentum operator and j_l and $h_l^{(1)}$ are, respectively, spherical Bessel and spherical Hankel functions of the first kind. The coefficients $A_{\rm E}(l,m)$ and $A_{\rm M}(l,m)$ determine the electric and magnetic multipole contributions of order l,m to the radiated power[25(a)]

$$P = \frac{c}{4\pi q^2}\sum_{lm}[|A_{\rm E}(l,m)|^2 + |A_{\rm M}(l,m)|^2]. \tag{11}$$

These coefficients are found in the forms

$$A_{\rm E}(l,m) = D_{\rm E}(l)d_{\rm E}(l,m), \tag{12a}$$

$$A_{\rm M}(l,m) = D_{\rm M}(l)d_{\rm M}(l,m), \tag{12b}$$

where

$$D_{\rm E}(l) = \frac{il}{x^2[\sqrt{\epsilon}j_l(x)h_l^{(1)\prime}(y) - j_l'(x)h_l^{(1)}(y) + (\sqrt{\epsilon}/y - 1/x)j_l(x)h_l^{(1)}(y)]}, \tag{13a}$$

$$D_{\rm M}(l) = \frac{i}{x^2}\frac{\sqrt{\epsilon}}{j_l(x)h_l^{(1)\prime}(y) - \sqrt{\epsilon}j_l'(x)h_l^{(1)}(y)}, \tag{13b}$$

and where $x=ka$ and $y=qa$. Primes denote derivatives. The coefficients $d_{\rm E}(l,m)$ and $d_{\rm M}(l,m)$ are obtained in terms of the source charge and current densities $\rho(\mathbf{r})$ and $J(\mathbf{r})$ [c.f. Ref. 25(a), Eqs. (16.91)–(92), modified for $\epsilon\neq 1$]

$$d_{\rm E}(l,m) = \frac{4\pi k^2}{i\sqrt{l(l+1)}}\int d\mathbf{r}\, Y_{lm}^*(\hat{r})\left\{\frac{1}{\sqrt{\epsilon}}\rho(\mathbf{r})\frac{\partial}{\partial r}(rj_l(kr)) + \frac{ik}{c}(\mathbf{r}\cdot\mathbf{J}(\mathbf{r}))j_l(kr)\right\}, \tag{14a}$$

$$d_{\rm M}(l,m) = \frac{4\pi k^2}{i\sqrt{\epsilon l(l+1)}}\int d\mathbf{r}\, Y_{lm}^*(\hat{r}) \times j_l(kr)\nabla\cdot\left(\frac{\mathbf{r}\times\mathbf{J}(\mathbf{r})}{c}\right), \tag{14b}$$

(here $\hat{r}\equiv(\vartheta,\varphi)$). For a point dipole at $\mathbf{r}=\mathbf{R}$ oscillating with frequency ω

$$\mathbf{J} = -i\omega\boldsymbol{\mu}\delta(\mathbf{r}-\mathbf{R}), \tag{15a}$$

$$\rho = -\boldsymbol{\mu}\cdot\nabla\delta(\mathbf{r}-\mathbf{R}). \tag{15b}$$

Using Eqs. (14) and (15) finally lead to

$$d_{\rm E}(l,m) = \frac{4\pi k^2}{i\sqrt{\epsilon}R^2}\left\{\boldsymbol{\mu}\cdot\mathbf{R}\sqrt{l(l+1)}Y_{lm}^*(\hat{R})j_l(z) + i\boldsymbol{\mu}\cdot\mathbf{R}\times\mathbf{X}_{lm}^*(\hat{R})\frac{d}{dz}[zj_l(z)]\right\}, \tag{16a}$$

$$d_{\rm M}(l,m) = \frac{4\pi ik^3}{\epsilon}\boldsymbol{\mu}\cdot\mathbf{X}_{lm}^*(\hat{R})j_l(z), \tag{16b}$$

where $z=kR$. Equation (12), (13), and (16) constitute the final results for the coefficients $A_{\rm E}(lm)$ and $A_{\rm M}'(lm)$ for the electromagnetic field outside the sphere [Eq. (10)]. Inserting these into Eq. (11) lead to

$$P=\frac{c}{8\pi q^2}\left[\sum_l |D_{\mathrm{E}}(l)|^2 \sum_m |d_{\mathrm{E}}(lm)|^2 + \sum_l |D_{\mathrm{M}}(l)|^2 \sum_m |d_{\mathrm{M}}(lm)|^2\right]. \quad (17)$$

Considerable simplification is achieved by averaging over all molecular orientations and over the angular part of the molecular position, thus replacing $\Sigma_m|d_{\mathrm{E}}(l,m)|^2$ and $\Sigma_m|d_{\mathrm{M}}(l,m)|^2$ by $(2l+1)\langle|d_{\mathrm{E}}(l,m)|^2\rangle$ and $(2l+1)\langle|d_{\mathrm{M}}(l,m)|^2\rangle$, respectively, (the averages do not depend on m). Using the identities

$$\langle(\mu\cdot\mathbf{a})\ (\mu\cdot\mathbf{b})\rangle_{\hat{\mu}}=\tfrac{1}{3}\mu^2\mathbf{a}\cdot\mathbf{b}, \quad (18)$$

$$\langle|Y_{lm}(R)|^2\rangle_{\hat{\mathbf{R}}}=\langle\mathbf{X}_{lm}(\hat{R})^*\cdot\mathbf{X}_{lm}(\hat{R})\rangle_{\hat{\mathbf{R}}}=\frac{1}{4\pi}, \quad (19)$$

we get

$$\langle|d_{\mathrm{E}}(l,m)|^2\rangle=\frac{4\pi\mu^2k^4}{36R^2}\left\{l(l+1)(j_l(z))^2+\left[\frac{d}{dz}(zj_l(z))\right]^2\right\}, \quad (20a)$$

$$\langle|d_{\mathrm{M}}(l,m)|^2\rangle=\frac{4\pi\mu^2k^\sigma}{3\epsilon^2}(j_l(z))^2. \quad (20b)$$

The averaged Eqs. (17) and Eqs. (20) now lead to the following expression for the averaged radiating power for a molecule (represented by an oscillating point dipole) located at a distance R from the sphere center

$$\langle P\rangle=\frac{c\mu^2k^4}{6}\sum_{l=1}^{\infty}(2l+1)\left\{\frac{1}{z^2}|D_{\mathrm{E}}(l)|^2\times\left[\left(\frac{d}{dz}(zj_l(z))\right)^2+l(l+1)(j_l(z))^2\right]+\frac{1}{\epsilon}|D_{\mathrm{M}}(l)|^2(j_l(z))^2\right\}\equiv P(z). \quad (21)$$

Note that the averages in Eqs. (20) and (21) are over $\hat{\mu}$ and $\hat{R}$, namely, over the molecular orientations and over a spherical shell of radius R about the sphere center. If we assume an homogeneous distribution, with density n, of molecules in the sphere, the total emitted power is obtained from

$$P^{\mathrm{tot}}=\frac{4\pi n}{k^3}\int_0^x dz\, z^2P(z), \quad (22)$$

where $x=ka$. This integral may be performed analytically, yielding

$$P^{\mathrm{tot}}=\frac{2}{3}\pi nc\mu^2k\sum_{l=1}^{\infty}\left\{|D_{\mathrm{E}}(l)|^2K_l+\frac{1}{\epsilon}|D_{\mathrm{M}}(l)|^2I_l\right\}, \quad (23)$$

$$K_l=x^2j_l(x)j_l'(x)+xj_l^2(x)+\frac{x^3}{2}[j_l(x)-j_{l-1}(x)j_{l+1}(x)], \quad (24a)$$

$$I_l=\frac{x^3}{2}[j_l^2(x)-j_{l-1}(x)j_{l+1}(x)]. \quad (24b)$$

Finally, the emitted power from a free molecule is given by [cf. Eq. (8) with $\epsilon=1$]

$$P_0=\frac{\omega^4\mu^2}{3c^3}. \quad (25)$$

Thus the ratio of the radiative emission rates may be obtained from $\Gamma(z)/\Gamma_0=P(z)/P_0$ and $\langle\Gamma\rangle/\Gamma_0=P^{\mathrm{tot}}/((4\pi a^3/3)nP_0)$. Note however that because cavity corrections are not included in the present discussion these ratios correspond to the f_s terms only. We get (letting $z=kR$)

$$f_s(z)=\frac{1}{2}\epsilon^2\sum_{l=1}^{\infty}(2l+1)\left\{\frac{1}{z^2}|D_{\mathrm{E}}(l)|^2\times\left[\left(\frac{d}{dz}(zj_l(z))\right)^2+l(l+1)(j_l(z))^2\right]+\frac{1}{\epsilon}|D_{\mathrm{M}}(l)|^2(j_l(z))^2\right\}, \quad (26)$$

and (letting $y=qa$)

$$\langle f_s\rangle=\frac{3\sqrt{\epsilon}}{2y^3}\sum_{l=1}^{\infty}(2l+1)\left(|D_{\mathrm{E}}(l)|^2K_l+\frac{1}{\epsilon}|D_{\mathrm{M}}(l)|^2I_l\right). \quad (27)$$

Equation (26) gives the ratio of radiative decay rate (relative to the free molecule, averaged over molecular orientations and without cavity corrections) for a molecule located at a distance R from the center of a sphere of radius a and a dielectric constant (at the molecular frequency ω) ϵ. Equation (27) is the average of this ratio over all R between 0 and a.

To end this section we note that in the small sphere limit $x,y\ll 1$, Eq. (26) may be shown to yield the electrostatic result (2). This electrostatic limit is obtained when $ka=\sqrt{\epsilon}qa\ll 1$, namely, when the particle size a is small relative to the radiation wavelength *in the particle*. Also we note that for $\epsilon=1$ Eqs. (13) become

$$|D_{\mathrm{E}}|^2=|D_{\mathrm{M}}|^2=1.$$

We have verified numerically that in this limit f_s, Eq. (26), and $\langle f_s\rangle$, Eq. (27), both become 1 as expected.

III. CAVITY CORRECTIONS

In the previous section we have modeled a fluorescing molecule in a dielectric solvent as a point dipole embedded in a continuous dielectric environment. This model completely ignores the molecular structure of the solvent. In this section we follow a common practice in rectifying this point by assuming that the molecule is enclosed in a cavity of size characteristic of the distance between the molecule and its nearest solvent neighbors. The value of ϵ inside the cavity is taken to be 1.

In the absence of evidence to the contrary, it is natural to assume that large atomic (e.g., rare gas and metal) clusters are approximately spherical. On the other hand, while most treatments of cavity models have considered spherical cavities, the shape of the cavity is actually determined by the embedded molecule. Mayers and Birge[10] have made the important observation that the orientation of the molecular transition dipole with respect to a nonspherical cavity is crucial in determining the fluorescence lifetime. They have considered cylindrical cavities and have shown that when the

molecular transition dipole is parallel to the cylinder axis the fluorescence lifetime is longer than that of the free molecule, while the opposite is true if the transition dipole is perpendicular to this axis.

To account for possible similar effects we will consider later cavities of spheroidal shapes. Also, we assume that the cavity size is much smaller than the cluster size. (Obviously it is much smaller than the radiation wavelength so an electrostatic treatment of the cavity is always possible.) To see the significance of this assumption consider first (Fig. 1) the case of a molecule (represented by a point dipole μ) at the center of a spherical cavity (radius r_0, dielectric constant ϵ_3), which is in turn located at the center of a small spherical particle (radius a and dielectric constant ϵ_2), all embedded in an infinite medium of dielectric constant ϵ_1. For $\epsilon_3 = 1$ and $\epsilon_2 = \epsilon_1 = \epsilon$ this corresponds to a point dipole inside a spherical cavity in an infinite dielectric medium. For $\epsilon_3 = \epsilon_1 = 1$ and $\epsilon_2 = \epsilon$ this corresponds to a similar situation in a finite dielectric sphere. In the electrostatic limit ($a \ll \lambda$) the radiative emission rate can be obtained by calculating the effective total dipole of the system. To do this we calculate (Appendix A) the electrostatic potential induced by the dipole μ at large distance from the center of the system in Fig. 1. This potential should be given by $\mu_{\text{eff}} \cdot \mathbf{r}/r^3$, giving μ_{eff} in the form $\mu_{\text{eff}} = f^{1/2}\mu$, where f is the factor relating the actual emission rate with the emission rate associated with the bare dipole. The result of this calculation (see Appendix A) is

$$f = \left(\frac{9\epsilon_1 \epsilon_2}{(\epsilon_3 + 2\epsilon_2)(\epsilon_2 + 2\epsilon_1) + 2(\epsilon_3 - \epsilon_2)(\epsilon_2 - \epsilon_1)(r_0/a)^3} \right)^2 . \tag{28}$$

The case of a dipole in a small sphere in the continuum limit (no cavity) is obtained by taking $\epsilon_3 = \epsilon_2 = \epsilon$ and $\epsilon_1 = 1$. This leads to

$$f = f_s \equiv \left(\frac{3}{\epsilon + 2} \right)^2 , \tag{29}$$

as before (Eq. 2). The cavity factor is obtained by taking $\epsilon_2 = \epsilon_1 = \epsilon$ and $\epsilon_3 = 1$. In this limit

$$f = f_c \equiv \left(\frac{3}{\epsilon^{-1} + 2} \right)^2 . \tag{30}$$

Physically, a model which accounts for the atomic nature of the solvent by considering a cavity in a continuum dielectric makes sense only if $r_0 \ll a$. In this limit and for $\epsilon_3 = \epsilon_1 = 1$; $\epsilon_2 = \epsilon$ Eq. (28) becomes

$$f = f_c f_s . \tag{31}$$

A simple interpretation of Eq. (31) is obtained by realizing (Appendix A) that the effective dipole associated with a dipole μ in a small spherical cavity inside a bulk dielectric solvent is $\mu_{\text{eff}} = f_c^{1/2}\,\mu$ (namely, the far field outside the cavity is that of a dipole μ_{eff}). In fact, in the limit $r_0 \ll a$ this is true for any cavity shape, and the factor f_c depends only on the cavity and not on the size and shape of the particle. To an observer far away from the cavity, the cavity containing the molecular dipole appears as such an effective point dipole. The radiative decay rate associated with this effective dipole is $\sim f_s |\mu_{\text{eff}}|^2$. We conclude that in the limit $r_0 \ll a$ the calculation of f can be separated into the calculation of the factor f_c which depends only on the cavity, and the factor f_s which depends only on the particle. This is the theoretical basis for Eq. (3). It should be stressed however that the result (30) is obtained by assuming that the molecular dipole is enclosed in a real cavity inside the dielectric continuum. If instead the molecule occupies a substitutional site of the solvent lattice the result is (for a cubic lattice)[15,26]

$$f_c = \left(\frac{\epsilon + 2}{3} \right)^2 . \tag{32}$$

For the experimental system considered here (DCA in Ar) a real cavity model seems more appropriate. Note that if Eqs. (29) and (32) are adopted, Eq. (31) yields $f = 1$, in contrast to the experimental observation.

To account for cavity shape dependence we next calculate cavity correction factors for spheroidal cavities. We consider a point dipole μ located in such a cavity (Fig. 2), where the dielectric constants are 1 inside and ϵ outside the cavity. An electrostatic calculation of the potential at large distance should yield again $\mu_{\text{eff}} \cdot \mathbf{r}/r^3$, leading to an expression for f_c from

$$f_c = \frac{|\mu_{\text{eff}}|^2}{|\mu|^2} . \tag{33}$$

Details of this calculation for both prolate and oblate[27] spheroidal cavities are described in Appendix B. Remarkably the results do not depend (in the electrostatic limit) on

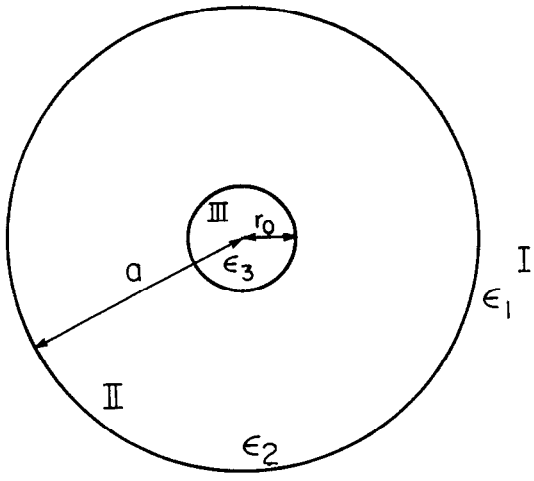

FIG. 1. A model for a spherical cluster with a spherical molecular cavity. In the present application $\epsilon_1 = \epsilon_3 = 1$ and $\epsilon_2 = \epsilon$ is the cluster dielectric constant.

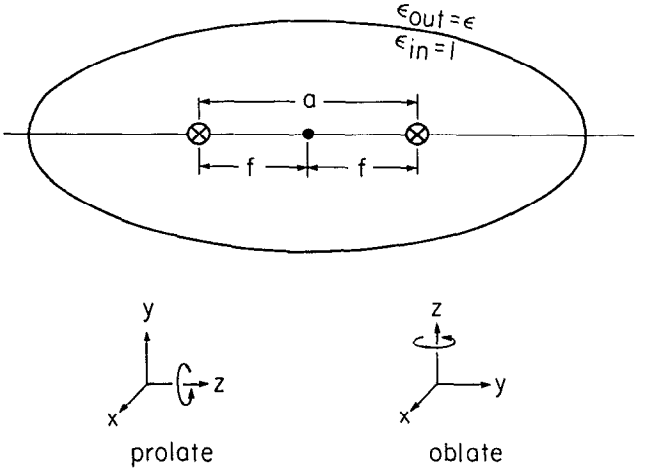

FIG. 2. A spheroidal cavity obtained by rotating the ellipse about the z axis.

the cavity size *and on the location of the dipole inside the cavity*. They do depend however on the cavity shape (i.e., the aspect ratio and the oblate and prolate symmetry) and on the *orientation* of the molecule relative to the spheroid axes. Let z be the symmetry axis (long and short axis for prolate and oblate spheroids, respectively) and take the molecular dipole to lie in the xz plane, namely, $\boldsymbol{\mu}=(\mu_x,0,\mu_z)$. Then

$$\mu_x^{\text{eff}}=f_{cx}^{1/2}\mu_x;\quad \mu_z^{\text{eff}}=f_{cz}^{1/2}\mu_z. \tag{34}$$

For a prolate spheroid defined in prolate spheroidal coordinates (ξ,η,ϕ) by $\xi=\xi_0$ (namely, the aspect ratio[25] is $\rho=(\xi_0^2-1)^{1/2}/\xi_0;\ \xi_0=1,\ldots,\infty$) the results are

$$f_{cx}^{1/2}=\frac{2}{\sqrt{\xi_0^2-1}((1/\epsilon)\xi_0 Q_1^1(\xi_0)-(\xi_0^2-1)Q_1^{1\prime}(\xi_0))} \tag{35}$$

and

$$f_{cz}^{1/2}=\frac{1}{(\xi_0^2-1)((1/\epsilon)Q_1^0(\xi_0)-\xi_0 Q_1^{0\prime}(\xi_0))}. \tag{36}$$

In these equations Q_1^0 and Q_1^1 are the Legendre functions

$$Q_1^0(Z)=\frac{1}{2}Z\log\left(\frac{Z+1}{Z-1}\right)-1, \tag{37a}$$

$$Q_1^1(Z)=(Z^2-1)^{1/2}\left[\frac{Z}{Z^2-1}-\frac{1}{2}\log\left(\frac{Z+1}{Z-1}\right)\right], \tag{37b}$$

and $Q'(Z)=dQ(Z)/dZ$. For an oblate spheroid defined by $\xi=\xi_0$ in oblate spheroidal coordinates (aspect ratio $\rho=\xi_0/(\xi_0^2+1)^{1/2};\ \xi_0=0,\ldots,\infty$) the results are

$$f_{cx}^{1/2}=\frac{2}{(1-1/\epsilon)[\xi_0^2-\xi_0(\xi_0^2+1)\text{arctg}(\xi_0^{-1})]+2}, \tag{38}$$

and

$$f_{cz}^{1/2}=\frac{1}{(1-1/\epsilon)(\xi_0^2+1)[\xi_0\,\text{arctg}(\xi_0^{-1})-1]+1}. \tag{39}$$

Numerical results based on Eqs. (35)–(36) and (38)–(39) are given in Sec. IV. The sphere limit is obtained by taking $\xi_0\to\infty$ in any of these equations. Using in this limit $Q_1^0(\xi_0)\to(3\xi_0^2)^{-1}$, $Q_1^1(\xi_0)\to 2(3\xi_0^2)^{-1}$ and $\text{arctg}(\xi_0^{-1})\to 1/\xi_0-1/(3\xi_0^3)+\cdots$ leads to Eq. (30).

IV. NUMERICAL RESULTS AND DISCUSSION

The radiative lifetime (and the associated oscillator strength) of excited molecules embedded in condensed environments has long been known to depend on the solvent and on the nature of the molecule solvent interaction. In this paper and in the previous papers of this series[2] we have focused on solvents of finite size, and have undertaken to elucidate within classical electrodynamics the *cluster size* dependence of this phenomenon.

Notwithstanding specific molecular interactions that will undoubtedly be found in particular systems, we have found that the cluster size dependence on the radiative lifetime of solute molecules behave differently in four different regimes:

(a) *The microscopic regime* (from 1 to a few tens of solvent molecules). For such cluster sizes the radiative lifetime depends strongly and specifically on the number of solvent atoms and on their specific positions (i.e., on the cluster structure).[2]

(b) *The electrostatic regime* (from $\sim 10^2$ solvent molecules up to cluster sizes of $\sim 0.1\lambda$, where λ is the wavelength of the emitted light). For such clusters a model involving a point dipole (representing the molecular transition dipole) in a dielectric cluster seems to account for the gross features of the observed behavior. For spherical and spheroidal clusters this model predicts that the effective radiative decay rate does not depend on the cluster size (in accord with experimental observations[2(b)]) and on the location of the molecule within the cluster.

(c) *The electrodynamic regime* (particles larger than $\sim 0.1\lambda$) where the radiative lifetime is again dependent on the particle size as well as on the molecular location and orientation.

(d) *The bulk regime* is realized for solvent particles much larger than λ. The radiative lifetime of molecules embedded in such particles is the same as in bulk, provided that the molecule is not too close to the particle surface.

This paper deals with the transition from the electrostatic to the bulk regime as obtained from classical electrostatics for spherical solvent particles. Our results are summarized in Figs. 3–6 which display the results obtained in Sec. II. It should be noted that these results are obtained in Sec. II in a model of a point dipole embedded in a dielectric solvent without any microscopic cavity. These are therefore just the f_s factors defined in Sec. I, namely, the relative radiative emission rates without cavity corrections. Model results for the cavity correction factors are presented later.

Figure 3 shows the f_s factor for a molecule represented by a point dipole located in the center of a dielectric sphere, as a function of the sphere size. We have chosen $\epsilon=1.63$, the dielectric constant of bulk Ar. Figure 3(a) shows this dependence on a linear scale while Fig. 3(b) shows the same results on a logarithmic scale. Figure 3(b) clearly exhibits the transition between the electrostatic and the electromagnetic regimes. In the former f_s is <0.7 and independent of

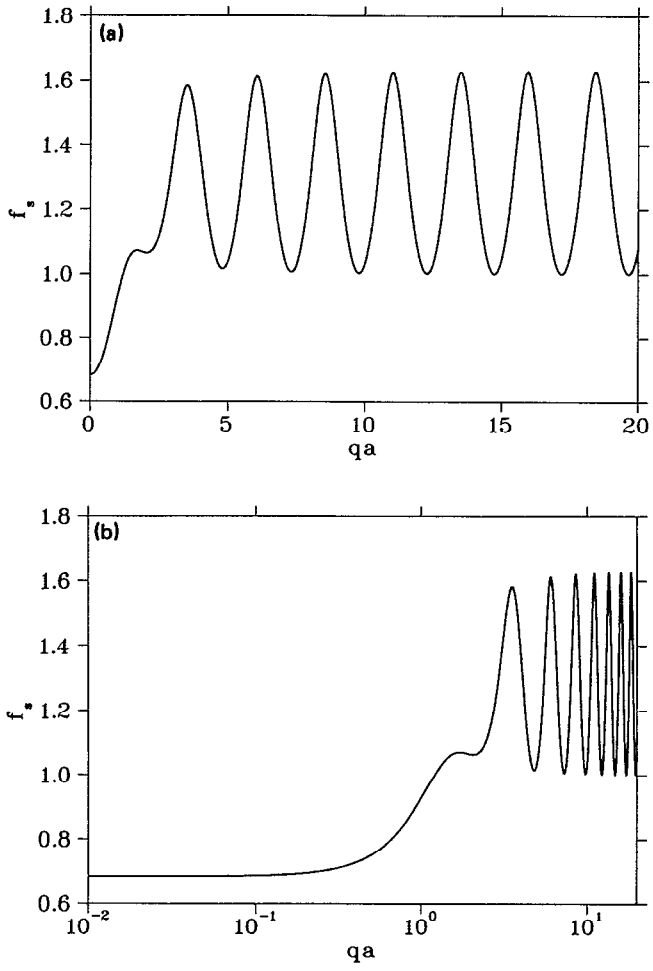

FIG. 3. The cluster contribution f_s to $f = \Gamma_R/\Gamma_R^0$ for a spherical cluster as a function of the cluster radius (in units of q^{-1}). The molecule is at the sphere center. $\epsilon = 1.63$ (Ar). (a) Linear, (b) logarithmic scale.

cluster size. In the latter f_s oscillates as a function of the radius about the bulk value ($\sqrt{1.63} = 1.28$) with a period π/k ($k = q\sqrt{\epsilon}$). Note that f_s *does not* go to the bulk value for this special geometry, but oscillates about it.

A simple expression for f_s in this situation may be obtained from Eq. (26), but more physical insight is gained by considering the following derivation: Starting from Eq. (6), assume that the point dipole is in the middle of a sphere of radius a and dielectric constant ϵ. The vector potential just out of the sphere may be written as

$$\mathbf{A} = -\frac{i\omega\mu e^{ika}}{ca}(T + Re^{2ika}T + R^2e^{4ika}T + \cdots) = -\frac{i\omega\mu e^{ika}}{ca}\frac{T}{1 - Re^{2ika}}, \tag{40}$$

where c is the speed of light and where R and T are the reflection and transmission coefficients, respectively, at the sphere boundary. Since the wave is spherical, $\mathbf{E}$ and $\mathbf{B}$ are parallel to the spherical interface, so R and T are given by the standard expressions for a beam normal to a planar interface

$$T = \frac{2\sqrt{\epsilon}}{1 + \sqrt{\epsilon}}, \tag{41}$$
$$R = \frac{1 - \sqrt{\epsilon}}{1 + \sqrt{\epsilon}}.$$

The vector potential for $r > a$ may also be written in terms of the effective dipole μ_{eff}

$$\mathbf{A} = -\frac{i\omega}{c}\frac{e^{iqr}}{r}\mu_{\text{eff}}, \tag{42}$$

from which we get

$$\mu_{\text{eff}} = \mu\frac{e^{i(k-q)a}T}{1 - Re^{2iqa}}. \tag{43}$$

Using Eq. (41) this leads to

$$f_s = \frac{|\mu_{\text{eff}}|^2}{|\mu|^2} = \frac{2}{1 + 1/\epsilon + (1 - 1/\epsilon)\cos(2ka)}. \tag{44}$$

Note that from $(2\pi)^{-1}\int_0^{2\pi}d\vartheta(1 - z\cos\vartheta)^{-1} = (1 - z^2)^{-1/2}$ it follows that the average of this result over a is indeed $\sqrt{\epsilon}$.

Figures 4 display the f_s factor averaged over a uniform distribution of molecules in the sphere and over a uniform distribution of molecular orientations [Eq. (27)], as a function of the sphere radius. In Fig. 4(a) (solid line) this is shown for $\epsilon = 1.63$, while Figs. 4(b) and 4(c) display similar results for $\epsilon = 3$, using linear and logarithmic scales, respectively. It is seen that the averaged emission rate associated with such a uniform distribution of molecules is characterized by a strong resonance structure as a function of sphere size. We note in passing that in any real experiment the resonance structure seen in Figs. 4 and 5 should be averaged over a distribution of cluster sizes and shapes. This will have the effect of reducing or eliminating the structure. This is shown in Fig. 4(a) which also displays results averaged over a Gaussian distribution of sphere sizes (namely, the size distribution about a is taken $P(a';a) \sim \exp[-(a' - a)^2/\Delta^2]$). The structure is seen to be largely eliminated when Δ is of order $0.5q^{-1}$, as may have been expected.

To understand the origin of this resonance structure we show in Figs. 5 the dependence of f_s on the radial distance of the molecule from the sphere center. These results are obtained by averaging over a uniform distribution of molecules in a spherical shell of radius R ($R < a$) about the sphere center, and over all molecular orientations [cf. Eq. (26)]. The dependence of f_s on $z = qR$ is shown in Figs. 5(a)–5(c) for three different sphere radii: In Fig. 5(a) $\epsilon = 1.63$ and $qa = 19.54$. For this ϵ, this choice of qa corresponds to the $M21$ resonance, namely, in Eq. (27) the term containing $D_{\text{M}}(21)$ dominates. In Fig. 5(b) $\epsilon = 3$ and $qa = 19.75$., corresponding to the $E24$ resonance [the term containing $D_{\text{E}}(24)$ dominates in Eq. (27)]. Finally in Fig. 5(c) $\epsilon = 1.63$ and $qa = 19.22$, which is an off resonance situation.

These figures show the sense in which the bulk limit is approached when the cluster size increases: Figs. 5 clearly show that this limit is quickly approached as the sphere radius becomes larger than the radiation wavelength—for molecules not in the surface region. Surface molecules strongly

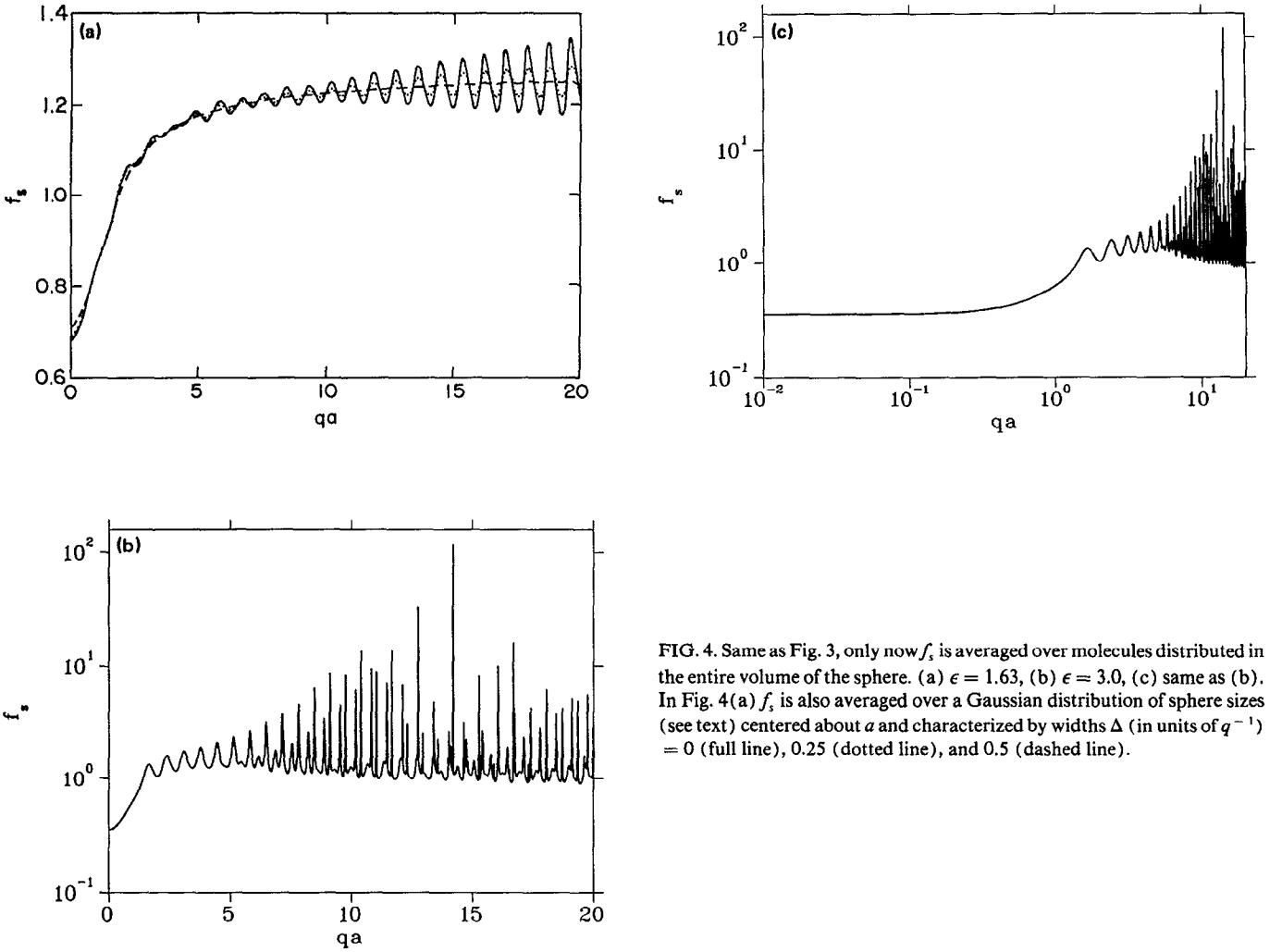

FIG. 4. Same as Fig. 3, only now f_s is averaged over molecules distributed in the entire volume of the sphere. (a) $\epsilon = 1.63$, (b) $\epsilon = 3.0$, (c) same as (b). In Fig. 4(a) f_s is also averaged over a Gaussian distribution of sphere sizes (see text) centered about a and characterized by widths Δ (in units of q^{-1}) $= 0$ (full line), 0.25 (dotted line), and 0.5 (dashed line).

interact with Mie resonances[18] of the electromagnetic field in the sphere. For large l values these resonances are essentially surface waves, associated with a standing wave structure within the circumference of the sphere (for example a ray forming a polygon due to total internal reflection from the spherical interface). When the sphere radius supports such a resonance (at the given frequency and for the given ϵ), molecules at the surface region interact strongly with this resonance and this gives rise to the enhanced radiative emission rate observed in Figs. 5(a) and 5(b). Away from resonance the surface field is weaker than in the bulk of the cluster because surface modes are not supported and radial modes suffer from partial destructive interference with waves reflected from the sphere surface. This gives rise to the lower surface emission rate seen in Fig. 5(c).

It is interesting to compare the Mie resonance structure seen in Fig. 4 for the emission rate from a uniform distribution of excited molecules inside the sphere, with corresponding structure of standard Mie scattering, namely, the light scattering cross section as a function of the sphere radius or of the inverse wavelength of the radiation field. Expressions for Mie scattering cross sections are available in, e.g., Refs. 18 and 24(a). The total scattering cross section is given by [cf. Ref. 24(a), Eq. (16.144)]

$$\sigma_{sc} = \frac{\pi}{2q^2} \sum_l (2l+1)(|\alpha(l)|^2 + |\beta(l)|^2), \tag{45}$$

$$\alpha(l) = \frac{\gamma(l) j_l(ka) - 2j_l(qa)}{h_l(qa)}, \tag{46a}$$

$$\beta(l) = \frac{\delta(l) j_l(ka) - 2j_l(qa)}{h_l(qa)}, \tag{46b}$$

where

$$\gamma(l) = \frac{2i}{qa}\left[\left(\frac{d}{dy}(yh_l(y))\right)_{y=qa} j_l(ka) - h_l(qa) \times \left(\frac{d}{dx}(xj_l(x))\right)_{x=ka}\right]^{-1}, \tag{47a}$$

$$\delta(l) = \frac{2i}{qa}\left[\left(\frac{d}{dy}(yh_l(y))\right)_{y=qa} j_l(ka) - \frac{1}{\epsilon} h_l(qa)\left(\frac{d}{dx}(xj_l(x))\right)_{x=ka}\right]^{-1}, \tag{47b}$$

(note that for $\epsilon = 1$, $k = q$, $\gamma = \delta = 2$ and $\alpha = \beta = 0$). Figures 6 display the Mie scattering cross section [Eq. (45)] as a function of qa, for spheres with $\epsilon = 1.63$ [Fig. 6(a)] and

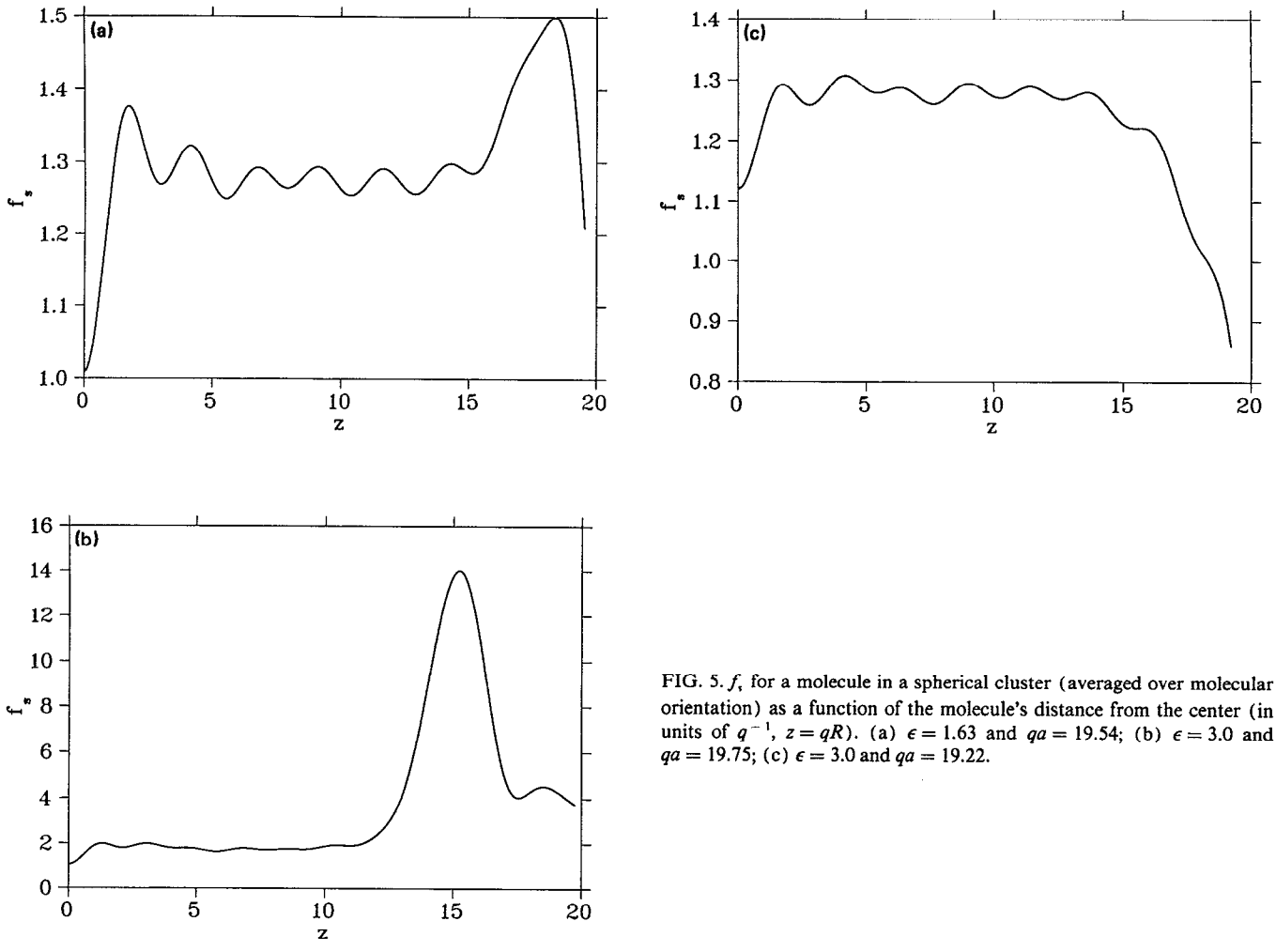

FIG. 5. f_s for a molecule in a spherical cluster (averaged over molecular orientation) as a function of the molecule's distance from the center (in units of q^{-1}, $z = qR$). (a) $\epsilon = 1.63$ and $qa = 19.54$; (b) $\epsilon = 3.0$ and $qa = 19.75$; (c) $\epsilon = 3.0$ and $qa = 19.22$.

$\epsilon = 3$ [Fig. 6(b)]. It is seen that the resonance structure of the Mie cross section is very different from that seen above for the radiative emission rate, the latter being much more structured. The origin of this difference lies in the fact that an incident electromagnetic field couples differently to the sphere eigenmodes than does an internal radiating dipole. For example those eigenmodes which in the limit of ray optics would appear as closed polygons due to total internal reflection from the sphere surface can not couple to an incident field but do couple to the internal dipole.

To complete the presentation of our results, we show in Figs. 7 the cavity correction factor f_c as a function of the aspect ratio ρ for spheroidal cavities. Figures 7(a) and 7(b) give results for prolate and oblate spheroidal shapes, respectively. z denotes the direction of the symmetry axis (long axis for a prolate spheroid, short axis for an oblate shape), and f_{cx} and f_{cz} correspond to molecules whose transition dipoles (represented by oscillating point dipoles) are in the x and z directions, respectively. It is interesting to note that in contrast to the results of Myers and Birge[10] (who studied the case of a cylindrical cavity), f_c for spheroidal cavities always remains larger than 1.

For $\rho = 1$ (spherical cavity) and $\epsilon = 1.63$ (solid argon) f_c [Eq. (30)] is 1.32, and with the electrostatic result for f_s [Eq. (2)] $= 0.68$, yield $f = f_c f_s = 0.9$, in very close agreement with experimental results for dichloroanthracene (DCA) in Ar,[2] as noted before. This agreement may be fortuitous though because, as seen from Figs. 7 f_c is sensitive to the cavity shape, and for a nonspherical cavity—to the molecule orientation within the cavity. For DCA, an oblate spheroidal cavity with the transition dipole in the x direction seems the best choice of the shapes considered here. We see from Fig. 7(b) that for this geometry f_c depends relatively weakly on the aspect ratio ρ. For $\rho = 0.5$ we get [Fig. 7(b)] $f_c \cong 1.2$, and $f = 0.82$, still in very close agreement with the results of Ref. 2(b).

A quantity closely related to the radiative emission rate of an excited molecule is the oscillator strength associated with the same molecular transition. The discussion of this subject in the literature is somewhat obscured by disagreements on the proper way to define the oscillator strength for a molecule interacting with its solvent environment. Without getting involved in these issues we limit ourselves to the following question: Does the ratio r between the *observed* radiative decay rate and between the *observed* integrated absorption line shape associated with the same molecular transition depend on cluster size? In our previous work[2(b)] we have found that in the electrostatic limit the answer is no. This result was obtained by observing that the cluster size dependence of the radiative emission rate is obtained from

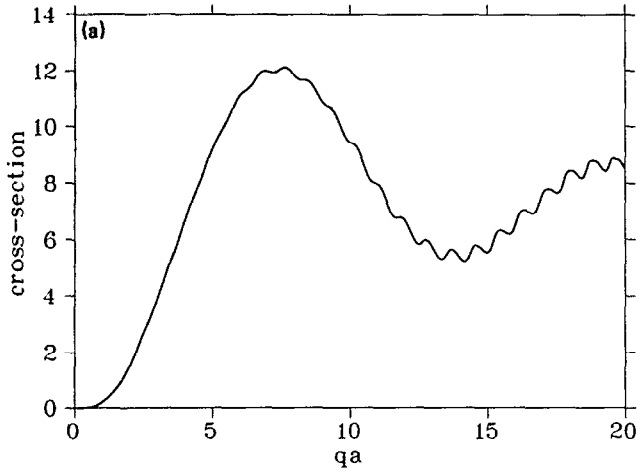

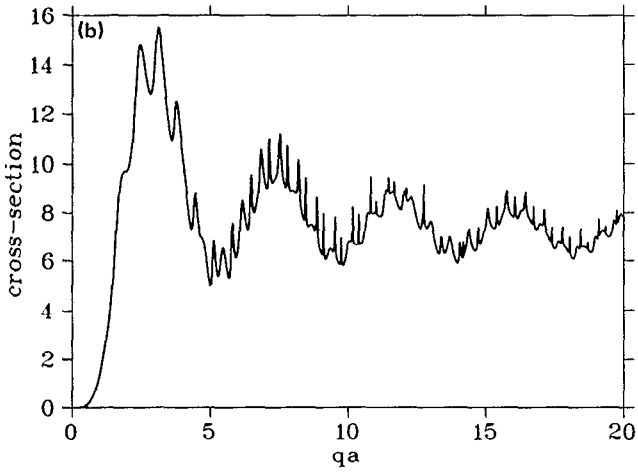

FIG. 6. Mie scattering cross section (in units of a^2) for a dielectric sphere as a function of size (in units of q^{-1}). (a) $\epsilon = 1.63$; (b) $\epsilon = 3.0$.

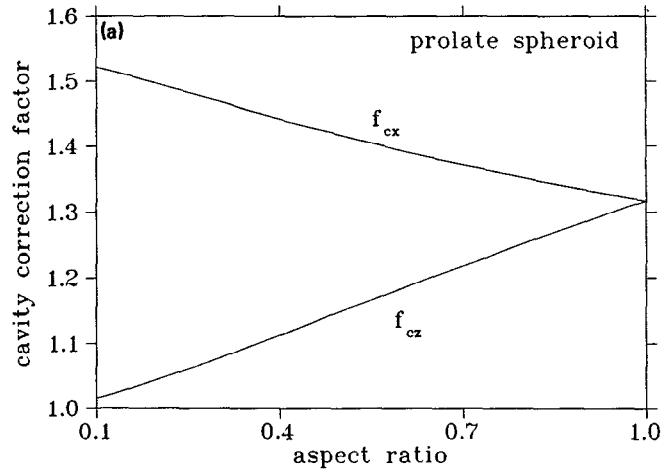

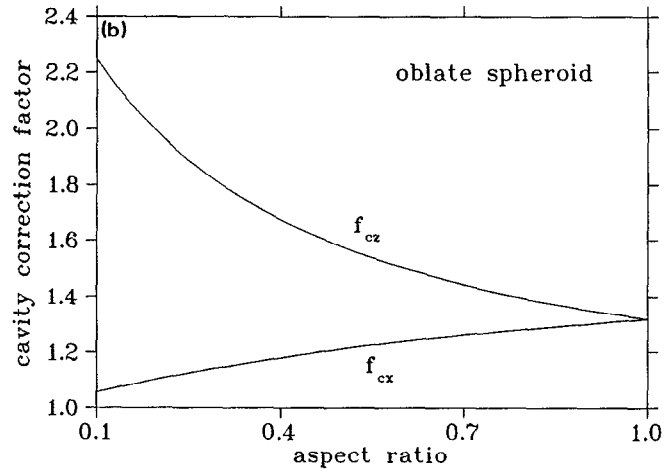

FIG. 7. Cavity corrections factors for a molecule in a spheroidal cavity. The dielectric constant of the environment is $\epsilon = 1.63$. f_{cx} corresponds to a molecule whose transient dipole is perpendicular to the symmetry axis of the spheroid. f_{cz} is for transition dipole parallel to the symmetry axis. (a) Prolate spheroid; (b) oblate spheroid.

the ratio $r_1 = (|\mu_{\text{eff}}|/|\mu|)^2$ while the cluster size dependence of the integrated absorption line shape is associated with the ratio $r_2 = (|E_{\text{loc}}|/|E_{\text{inc}}|)^2$, where E_{inc} is the incident field and E_{loc} is the local field at the position of the molecular transition dipole (represented by μ). In the electrostatic limit we have found that $r_1 = r_2$, thus $r = r_1/r_2$ is independent of cluster size. In the present electrodynamic calculation, the local field associated with a given incident electromagnetic field is obtained during the evaluation of the cross section for Mie scattering.[18] It can be shown that also in this general case r_1/r_2 is cluster size independent. Thus the *relation between the radiative emission rate and the integrated absorption line shape is cluster size independent for spherical clusters of arbitrary sizes.*

This paper has focused on the cluster size dependence of the radiative emission rate of an embedded molecule. Obviously a related subject of interest is the cluster size dependence of the level shift induced by the solvent environment. Experiment[2(b)] shows that in contrast to the radiative emission rate, the level shift approaches its bulk solvent limit already for clusters of ~50–100 solvent molecules, about the beginning of the electrostatic regime. This behavior can be easily rationalized within classical electrostatic theory: Solvent induced shifts are associated either with electrostatic solvation energies, when the electronic states involved are associated with different permanent charge distributions, or with dispersion energies related to the molecular polarizabilities associated with these electronic states. We shall now show that both effects saturate at relatively small cluster sizes.

Consider first the solvation energy of a point charge q or a point dipole μ located at the center of a spherical cavity of radius r_0. In a bulk solvent characterized by a dielectric constant ϵ, the Born solvation energy is

$$W = -\frac{q^2}{2r_0}\left(1 - \frac{1}{\epsilon}\right), \tag{48}$$

for a point charge, and

$$W = -\frac{\mu^2}{r_0^3}\frac{\epsilon - 1}{2\epsilon + 1}, \tag{49}$$

for a point dipole. These results are easily obtained using the electrostatic relation for polarization energy

$$W = -\frac{1}{2}\int_V d^3r\, \mathbf{P}\cdot\mathbf{E}_0, \tag{50}$$

where $\mathbf{E}_0$ is the bare (in the absence of the dielectric) field resulting from the given charge distribution, and where $\mathbf{P}$ is the polarization, related to the actual local field $\mathbf{E}$ by $\mathbf{P}=[(\epsilon-1)/4\pi]\mathbf{E}$. The integral is over the entire space. Equation (50) can be also used to obtain the solvation energy in a finite size dielectric particle. For the model of Fig. 1, using the local field calculated in Appendix A we get (for $\epsilon_3=\epsilon_1=1, \epsilon_2=\epsilon$)

$$W=-\frac{q^2}{2}\left(\frac{1}{r_0}-\frac{1}{a}\right)\left(1-\frac{1}{\epsilon}\right) \tag{51}$$

and

$$W=-\frac{\mu^2(\epsilon-1)}{2\epsilon+1+[2r_0^3(\epsilon-1)^2/a^3(\epsilon+2)]}\times\left(\frac{1}{r_0^3}-\frac{1}{a^3}\right), \tag{52}$$

for a point charge and a point dipole, respectively. It is seen that the bulk limit of these expressions is obtained for $a\gg r_0$. For the more relevant case of a solvated dipole the bulk limit is obtained for $(a/r_0)^3\gg 1$, namely, $a\geqslant 10-15$ Å (a few tens of small solvent molecules) if $r_0\sim 5A^0$.

Consider now the dispersion energy. This part of the level shift, which may be dominant if the electronic states involved are not associated with permanent dipoles, arises from correlated polarization fluctuations in the molecule and the solvent. Its calculation is related to, and is as intricate as the calculation of van der Waals forces.[28] A simple derivation for a two level molecule can be obtained using the Drude model, representing the molecular transition dipole by a classical oscillating (with the transition frequency ω) dipole μ, interacting with the polarizable solvent.[2,29,30] This leads[31,32] to the following result for the frequency shift $\Delta\omega$:

$$\frac{\Delta\omega}{\omega_0}=-\frac{\alpha}{2\mu}Re(E_{\mathbf{R}}), \tag{53}$$

where ω_0 is the bare (isolated molecule) transition frequency, α is the molecular polarizability and $E_{\mathbf{R}}$ is the reaction field from the polarized solvent. (Note that $E_{\mathbf{R}}$ is proportional to μ.) For the model of Fig. 1 $E_{\mathbf{R}}$ can be calculated from the formalism of Appendix A. This leads to (for $\epsilon_1=\epsilon_3=1, \epsilon_2=\epsilon$)

$$\frac{\Delta\omega}{\omega_0}=\left[-\frac{2\alpha}{r_0^3}\frac{\epsilon-1}{2\epsilon+1}\right]\times\frac{1-(r_0/a)^3}{1-2(r_0/a)^3[(\epsilon-1)^2/(\epsilon+2)(2\epsilon+1)]}.$$

We see also here that the bulk limit is approached for $a\gg r_0$. Note that the factor in square brackets is the bulk ($a\to\infty$) limit of this red shift. Thus the second factor determines the approach to this limit.

V. CONCLUSIONS

The radiative emission by an excited molecule imbedded in a dielectric environment is modified by the solvent host in a way which depends on the host dielectric response and on the shape and orientation (relative to the molecular transition dipole) of the small cavity surrounding the molecule. When the size of this cavity is far smaller then the size of the host cluster the radiative emission rate is multiplied by a factor $f=f_sf_c$, itself a product of the solvent factor f_s and the cavity factor f_c. This paper discusses both effects. We have extended previous calculations of the cavity factor (which does not depend on the size and shape of the host cluster), to include spheroidal cavity shapes. f_c can be larger or smaller then 1, depending on the cavity shape and on the molecule orientation in the cavity. Remarkably, f_c does not depend on the molecule location within the cavity in the physically relevant electrostatic limit. Also, for spheroidal geometry f_c was found to be always larger than 1.

For the solvent factor f_s we have identified four regimes of cluster size: The microscopic regime (up to a few tens of solvent molecules) in which f_s is sensitive to details of the cluster structure; the electrostatic regime (size much smaller than the wavelength λ in the cluster) where f_s follows the predictions of classical electrostatics, is independent of cluster size, and is smaller than unity; the elctrodynamic regime (size $\sim\lambda$) where f_s is dominated by electromagnetic (Mie) resonances in the particle and the bulk regime (size $\gg\lambda$) where molecules in the interior of the cluster behave as in infinite bulk [however molecules close (within distance λ) to the surface are still strongly affected by surface electromagnetic resonances].

This cluster size dependence of the radiative decay rate is in marked contrast to the size dependence of the shift in the transition frequency. Both shifts originated from solvation of permanent charge distributions, or with dispersion energy, approach the bulk limit when the cluster size becomes large relative to characteristic molecular size (which determine the cavity size).

Finally, the ratio between the observed integrated absorption lineshape ("oscillator strength") and the radiative decay rate is predicted not to depend on cluster size.

The results of this work has immediate implications for recent experimental work. The radiative lifetime of dichloroanthracene in intermediate size Ar cluster is in close agreement with the result of the present model, based on a spherical cluster and assuming that the molecule is surrounded by a small spheroidal cavity. It should be kept in mind however that the cavity model is only a simplified way of taking into account the discrete nature of the host, and that the choice of its shape is based on qualitative arguments.

For molecules imbedded in large dielectric particles, the observation that Mie resonances affect mainly molecules near the particle surface suggests a connection to the experimental observation by Chang and co-workers[31] that nonlinear optical effects involving dye molecules in small dielectric droplets are enhanced, and that the enhanced response is associated again with surface molecules. As already pointed out, this results from the large amplitude of the Mie resonances at the surface of large spherical particles.

ACKNOWLEDGMENTS

This work was supported in part by the U.S.-Israel Binational Science Foundation. We thank Professor Aviv Amirav for many illuminating discussions on both experimental and theoretical issues. We also thank Dr. Louis Brus,

Professor Joshua Jortner, and Professor Eric Weitz for many helpful discussions.

APPENDIX A: A SPHERICAL CAVITY IN A SPHERICAL CLUSTER

For the model of Fig. 1, the electrostatic potential in regions I, II, and III can be written by expanding the solution of the Laplace equation in spherical coordinates, taking into account that the potential in region I should vanish at infinite distance, and that the homogeneous part of the potential in region III has to be analytic at the origin. The nonhomogeneous part of the potential in region III arises from the point dipole at the center.

The general solution of the Laplace equation in spherical coordinates is

$$\Phi=\sum_{l=0}^{\infty}\sum_{m=-l}^{l}\left[A_{lm}r^{l}Y_{lm}(\vartheta,\phi)+B_{lm}r^{-(l+1)}Y_{lm}(\vartheta,\phi)\right]. \tag{A1}$$

The effective dipole μ_{eff} of this system is determined by the requirement that in the limit $r\to\infty$ the potential is

$$\Phi\to\mu_{\text{eff}}\cdot\mathbf{r}/r^{3}. \tag{A2}$$

We take the dipole to be in the z direction. It is therefore sufficient to consider the $l=1$, $m=0$ terms in the continuity conditions. We thus take

$$\Phi_{\text{I}}=\frac{A\cos\vartheta}{\epsilon_1 r^{2}}, \tag{A3}$$

$$\Phi_{\text{II}}=\frac{B\cos\vartheta}{r^{2}}+Cr\cos\vartheta, \tag{A4}$$

$$\Phi_{III}=\frac{\mu\cos\vartheta}{\epsilon_3 r^{2}}+Dr\cos\vartheta. \tag{A5}$$

The coefficients A,B,C, and D are obtained from the electrostatic continuity conditions at the boundaries $r=a$ (between regions I and II), and $r=r_0$ (between regions II and III). In particular, the result for the coefficient A is the desired expression for the effective dipole. We get $\mu_{\text{eff}}=f^{1/2}\mu$, with f given by Eq. (28). The gradient of Φ_{II} is used (after B and C are found) as the local field $\mathbf{E}$ needed to calculate the polarization $\mathbf{P}$ used in Eq. (50). The coefficient D is related to the reaction field at the molecule, needed for the calculation of the dispersion shift, Eq. (53).

APPENDIX B: SPHEROIDAL CAVITIES

Here we outline the derivation of Eqs. (35)–(39). Consider first prolate spheroidal cavity ($\epsilon=1$) in an infinite dielectric medium with dielectric constant ϵ. The coordinate system is chosen so that the z axis is the symmetry axis of the spheroid which is in this case also the direction of the long axis. The center of the spheroid is at the origin and the focal points are located at equal distances $f=0.5a$ from it. Prolate spheroidal coordinates (ξ,η,ϕ) are defined by

$$\xi=\frac{1}{a}\left(\sqrt{(z+a)^2+x^2+y^2}+\sqrt{(z-a)^2+x^2+y^2}\right), \tag{B1a}$$

$$\eta=\frac{1}{a}\left(\sqrt{(z+a)^2+x^2+y^2}-\sqrt{(z-a)^2+x^2+y^2}\right), \tag{B1b}$$

$$\phi=\operatorname{arctg}(y/x). \tag{B1c}$$

The inverse transformation is

$$x=\tfrac{1}{2}a\sqrt{(\xi^2-1)(1-\eta^2)}\cos\phi, \tag{B2a}$$

$$y=\tfrac{1}{2}a\sqrt{(\xi^2-1)(1-\eta^2)}\sin\phi, \tag{B2b}$$

$$z=\tfrac{1}{2}a\xi\eta. \tag{B2c}$$

ξ varies between 1 and $+\infty$, η — between -1 and 1 and ϕ between 0 and 2π. We consider a cavity defined by $\xi=\xi_0$. This corresponds to an aspect ratio $b_s/b_l=(\xi_0^2-1)^{1/2}/\xi_0$.

Let the point dipole be located at coordinates $\mathbf{r}_d=(\xi_d,\eta_d,\phi_d)$ inside the cavity. The Coulomb potential due to this dipole at ξ, $\xi_d\leqslant\xi\leqslant\xi_0$, is

$$\Phi_d=\mu\cdot\nabla_d\frac{1}{|\mathbf{r}-\mathbf{r}_d|}, \tag{B3}$$

where ∇_d is the gradient with respect to the dipole coordinates. The Greens function of the Laplace equation in prolate spheroidal coordinates is[32]

$$\begin{aligned}\frac{1}{|r-r_d|}=\frac{1}{f}\sum_{n=0}^{\infty}(2n+1)\sum_{m=0}^{n}\epsilon_m i^m\left[\frac{(n-m)!}{(n+m)!}\right]^2\\ \times\cos[m(\phi-\phi_d)]\\ \times P^m(\eta)P^m(\eta)P^m(\xi)Q^m(\xi),\end{aligned} \tag{B4}$$

where P_n^m and Q_n^m are Legendre functions of the first and second kind, respectively, and where $\epsilon_0=1$ and $\epsilon_m=2$ for $m\geqslant 1$. The potentials Φ_{in} ($\xi\leqslant\xi_0$) and Φ_{out} ($\xi\geqslant\xi_0$) are written in the forms

$$\begin{aligned}\Phi_{\text{in}}=\Phi_d+\sum_{n=0}^{\infty}\sum_{m=0}^{n}(C_{nm}\cos(m\phi)\\ +S_{nm}\sin(m\phi))P_n^m(\eta)P_n^m(\xi),\end{aligned} \tag{B5}$$

$$\begin{aligned}\Phi_{\text{out}}=\sum_{n=0}^{\infty}\sum_{m=0}^{n}(\gamma_{nm}\cos(m\phi)+\sigma_{nm}\sin(m\phi))\\ \times P_n^m(\eta)Q_n^m(\xi).\end{aligned} \tag{B6}$$

Because of the orthogonality of the P_n^m functions with different n or m, and because we are interested in the behavior of the potential as $\xi\to\infty$ where only $n=1$ terms are expected to contribute, it is enough to consider only such terms. The expressions for $n=1$ Legendre functions are[33]

$$P_1^0(Z)=Z, \tag{B7a}$$

$$P_1^1(Z)=\begin{cases}\sqrt{1-Z^2}, & Z<1,\\ -i\sqrt{Z^2-1}, & Z>1,\end{cases} \tag{B7b}$$

$$Q_1^0(Z)=\frac{1}{2}Z\log\frac{Z+1}{Z-1}-1 \tag{B7c}$$

$$Q_1^1(Z)=\sqrt{Z^2-1}\left[\frac{Z}{Z^2-1}-\frac{1}{2}\log\frac{Z+1}{Z-1}\right]\Bigg\}Z>1. \tag{B7d}$$

It is also useful to consider the asymptotic ($Z\to\infty$) behavior of the Q functions:

$$Q_1^0(Z)\to(3Z^2)^{-1},\quad Q_1^1(Z)\to 2(3Z^2)^{-1}. \tag{B8}$$

The continuity equations $[\Phi_{in}(\xi_0)=\Phi_{out}(\xi_0)$, $\Phi'_{in}(\xi_0)=\epsilon\Phi'_{out}(\xi_0)]$ written for $n=1$ and $m=0,1$ are

$$\frac{3}{f}\mu\cdot\nabla_d[P_1^0(\eta_d)P_1^0(\xi_d)]Q_1^0(\xi_0)+C_{10}P_1^0(\xi_0)=\gamma_{10}Q_1^0(\xi_0), \tag{B9a}$$

$$\frac{3}{f}\mu\cdot\nabla_d[P_1^0(\eta_d)P_1^0(\xi_d)]Q_1^{0\prime}(\xi_0)+C_{10}P_1^{0\prime}(\xi_0)=\epsilon\gamma_{10}Q_1^{0\prime}(\xi_0), \tag{B9b}$$

$$\frac{3i}{2f}\mu\cdot\nabla_d[\cos(\phi_d)P_1^1(\eta_d)P_1^1(\xi_d)]Q_1^1(\xi_0)+C_{11}P_1^1(\xi_0)=\gamma_{11}Q_1^1(\xi_0), \tag{B10a}$$

$$\frac{3i}{2f}\mu\cdot\nabla_d[\cos(\phi_d)P_1^1(\eta_d)P_1^1(\xi_d)]Q_1^{1\prime}(\xi_0)+C_{11}P_1^{1\prime}(\xi_0)=\epsilon\gamma_{11}Q_1^{1\prime}(\xi_0). \tag{B10b}$$

The equations for S_{11} and σ_{11} are identical to those [Eq. (B10)] for C_{11} and γ_{11}. These equations are simplified by using the following identities:

$$\mu\cdot\nabla_d[P_1^0(\eta_d)P_1^0(\xi_d)]=\frac{\mu_z}{f}, \tag{B11}$$

$$\mu\cdot\nabla_d[\cos(\phi_d)P_1^1(\eta_d)P_1^1(\xi_d)]=-i\frac{\mu_x}{f}. \tag{B12}$$

Equations (B7)–(B10) lead to the following results for γ_{10} and γ_{11}:

$$\gamma_{10}=\frac{3\mu_z}{\epsilon f^2}\frac{P_1^0(\xi_0)Q_1^{0\prime}(\xi_0)-P_1^{0\prime}(\xi_0)Q_1^0(\xi_0)}{P_1^0(\xi_0)Q_1^{0\prime}(\xi_0)-(1/\epsilon)P_1^{0\prime}(\xi_0)Q_1^0(\xi_0)}, \tag{B13}$$

$$\gamma_{11}=\frac{3\mu_x}{2\epsilon f^2}\frac{P_1^1(\xi_0)Q_1^{1\prime}(\xi_0)-P_1^{1\prime}(\xi_0)Q_1^1(\xi_0)}{P_1^1(\xi_0)Q_1^{1\prime}(\xi_0)-(1/\epsilon)P_1^{1\prime}(\xi_0)Q_1^1(\xi_0)}. \tag{B14}$$

For large ξ, the potential Φ_{out} is dominated by the $n=1$ terms in Eq. (B6). For μ in the z direction it is the $m=0$ term and we get

$$\Phi_{out}\overset{\xi\to\infty}{\to}\frac{\gamma_{10}f^2z}{3r^3}, \tag{B15}$$

where we have used Eq. (B2c), Eq. (B6), and the fact that for $\xi\to\infty$ ξ becomes identical to r/f. This in turn should be equal to $\mu_{eff}^z z/(\epsilon r^3)$, which provides a relation between γ_{10} and the z component of μ_{eff}. From Eqs. (B13) and (B15) we get after some algebra the final result, Eq. (36), for the relation between μ_z and μ_{eff}^z. Similarly, if the molecular dipole is in the x direction, we get

$$\Phi_{out}\overset{\xi\to\infty}{\to}\frac{2\gamma_{11}f^2x}{3r^3}=\frac{\mu_{eff}^x x}{r^3}, \tag{B16}$$

leading to Eq. (35) for μ_{eff}^x/μ_x.

The derivation of Eqs. (38) and (39) for the f_c factors in the case of oblate spheroidal cavities proceed along similar lines. Oblate spheroidal coordinates are related to cartesian coordinates by[28]

$$x=a\sqrt{(\xi^2+1)(1-\eta^2}\cos\phi, \tag{B17a}$$

$$y=a\sqrt{(\xi^2+1)(1-\eta^2}\sin\phi, \tag{B17b}$$

$$z=a\xi\eta, \tag{B17c}$$

$\xi=0,\ldots,\infty$, $\eta=-1,\ldots,1$ and $\phi=0,\ldots,2\pi$. z is the symmetry axis of the spheroid. In the present case this is also the direction of the short axis of the spheroid. The Green's function in these coordinates is (for $\xi>\xi_d$)

$$\frac{1}{|\mathbf{r}-\mathbf{r}_d|}=\frac{1}{a}\sum_{n=0}^{\infty}(2n+1)\sum_{m=0}^{n}\epsilon_m i^{m+1}\left[\frac{(n-m)!}{(n+m)!}\right]^2\times\cos[m(\phi-\phi_d)]P_n^m(\eta_d)\times P_n^m(\eta)P_n^m(i\xi_d)Q_n^m(i\xi). \tag{B18}$$

The oblate spheroid is defined by $\xi=\xi_0$, implying an aspect ratio $b_s/b_l=\xi_0/(\xi_0^2+1)^{1/2}$. The potential in and out of the cavity is given by an expansion similar to Eqs. (B5)–(B6), where Φ_d is given by Eqs. (B3) and (B18). Here we encounter Legendre functions of imaginary argument. In particular, the functions of the second kind are easily shown to satisfy

$$\begin{aligned}Q_0^0(iZ)&=-i\,\mathrm{arctg}(1/Z),\\ Q_1^0(iZ)&=Z\,\mathrm{arctg}(1/Z)-1,\\ Q_1^1(iz)&=(Z^2+1)^{1/2}\left(\frac{Z}{Z^2+1}-\mathrm{arctg}(1/Z)\right).\end{aligned} \tag{B19}$$

These functions, and the corresponding P functions are the only ones needed for the present analysis because the desired potential for $\xi\to\infty$ is dominated, as before, by $n=1$ terms. Repeating a procedure similar to that described for the prolate spheroid case, we finally arrive at Eqs. (38)–(39).

[1] See, e.g., *The Chemical Physics of Solvation*, edited by R. R. Dogonadze, E. Kalman, A. A. Kornyshev, and J. Ulstrup (Elsvier, Amsterdam, 1986), Part B.
[2] (a) N. Liver, A. Nitzan, A. Amirav, and J. Jortner, J. Chem. Phys. **88**, 3516 (1988); (b) A. Penner, A. Amirav, J. Jortner, A. Nitzan, and J. I. Gersten, *ibid.* **93**, 147 (1990).
[3] E. Shalev, N. Ben-Horin, U. Even, and J. Jortner (unpublished).
[4] I. B. Perlman, *Handbook of Fluorescence Spectra of Aromatic Molecules* (Academic, New York, 1965).
[5] N. Q. Chako, J. Chem. Phys. **2**, 644 (1934).
[6] D. L. Dexter, Solid State Phys. **6**, 253 (1958).
[7] R. L. Fulton, J. Chem. Phys. **61**, 4141 (1974).
[8] G. Nienhuis and C. Th. J. Alkemade, Physica **81C**, 181 (1976).
[9] S. Hirayama and D. Phillips, J. Photochem. **12**, 139 (1980).
[10] B. Myers and R. R. Birge, J. Chem. Phys. **73**, 5314 (1980).
[11] E. P. Gibson and A. J. Restl, Chem. Phys. Lett. **73**, 294 (1980).
[12] R. A. Lampert, S. R. Meech, J. Metcalfe, D. Phillips, and A. P. Schaap, Chem. Phys. Lett. **94**, 137 (1983).
[13] T. Shibuyal, J. Chem. Phys. **78**, 5175 (1983).
[14] T. Abe and I. Iweibo, J. Chem. Phys. **83**, 1546 (1985).
[15] J. Knoester and S. Mukamel, Phys. Rev. A **40**, 7065 (1989).
[16] See Sec. II. For a quantum mechanical derivation see Ref. 8.
[17] C. Crépin and A. Tramer, Chem. Phys. Lett. **170**, 446 (1990).
[18] B. Mie, Ann. Phys. (Leipzig) **25**, 377 (1908). For modern reviews, see M. Born and E. Wolf, *Principle of Optics* (Pergamon, Oxford, 1975); M. Kerker, *The Scattering of Light and Other Electromagnetic Radiation* (Academic, New York 1969).
[19] B. van der Pol and H. Bremmer, Philos. Mag. **24**, 141 (1937).
[20] H. Chew, P. J. McNulty, and M. Kerker, Phys. Rev. A **13**, 396 (1976).
[21] R. Ruppin, J. Chem. Phys. **76**, 1681 (1982).
[22] H. Chew, J. Chem. Phys. **87**, 1355 (1987).
[23] P. T. Leung and T. F. George, J. Chem. Phys. **87**, 6722 (1987).
[24] S. C. Ching, H. M. Lai, and K. Young, J. Opt. Soc. Am. B **4**, 1995 (1987); **4**, 2004 (1987).
[25] (a). J. D. Jackson, *Classical Electrodynamics* (Wiley, New York, 1975),

Chap. 16; (b) Ref. 23(a), Eq. (6.62) modified for $\epsilon \neq 1$.
[26] M. Agranovich and M. D. Galanin, *Electronic Excitation Energy Transfer in Condensed Matter*, edited by V. M. Agranovich and A. A. Maradudin (North Holland, Amsterdam, 1982).
[27] A Prolate spheroid is obtained by rotating an elipse about the long axis. An oblate spheroid is obtained by rotating it about the short axis. The aspect ratio is the ratio between the short and long axes of the spheroid.
[28] Yu. S. Barash and V. L. Ginzburg, Usp. Fiz. Nauk **143**, 345 (1984) [Sov. Phys. Usp. **27**, 467 (1984)].
[29] R. R. Chance, A. Prock, and R. Silbey, Adv. Chem. Phys. **37**, 1 (1978).
[30] J. I. Gersten and A. Nitzan, J. Chem. Phys. **75**, 1139 (1981).
[31] S.-X. Qian, J. B. Snow, H. M.-Tzeng and R. K. Chang, Science **231**, 486 (1986).
[32] P. M. Morse and H. Feshbach, *Methods of Theoretical Physics* (McGraw-Hill, New York, 1953).
[33] Sign conventions for P^1 and Q^1 follow Ref. 26, and are somewhat different from those in Jackson (or in Abramovitz and Stegun). The final results are of course invatiant to these conventions.